Piezoelectric Floating Element Shear Stress Sensor for the Wind Tunnel Flow Measurement

Taeyang Kim, Aditya Saini, Jinwook Kim, *Student Member, IEEE*, Ashok Gopalarathnam, Yong Zhu, Frank L. Palmieri, Christopher J. Wohl, and Xiaoning Jiang, *Senior Member, IEEE*

***Abstract*—A piezoelectric (PE) sensor with a floating element was developed for direct measurement of flow induced shear stress. The PE sensor was designed to detect the pure shear stress while suppressing the effect of normal stress generated from the vortex lift up by applying opposite poling vectors to the PE elements. During the calibration stage, the prototyped sensor showed a high sensitivity to shear stress (91.3 $\pm$ 2.1 pC/Pa) due to the high PE coefficients ($d_{31} = -1330$ pC/N) of the constituent 0.67Pb($Mg_{1/3}Nb_{2/3}$)O_3–0.33$PbTiO_3$ (PMN–33%PT) single crystal. By contrast, the sensor showed almost no sensitivity to normal stress (less than 1.2 pC/Pa) because of the electromechanical symmetry of the sensing structure. The usable frequency range of the sensor is up to 800 Hz. In subsonic wind tunnel tests, an analytical model was proposed based on cantilever beam theory with an end-tip-mass for verifying the resonance frequency shift in static stress measurements. For dynamic stress measurements, the signal-to-noise ratio (SNR) and ambient vibration-filtered pure shear stress sensitivity were obtained through signal processing. The developed PE shear stress sensor was found to have an SNR of 15.8 $\pm$ 2.2 dB and a sensitivity of 56.5 $\pm$ 4.6 pC/Pa in the turbulent flow.**

***Index Terms*—Bimorph piezoelectric (PE) structures, electromechanical symmetry, floating element (FE), PMN–33%PT crystal, shear stress.**

I. Introduction

THE measurement of wall shear stress due to flow past solid surfaces provides important information about flow phenomena, including viscous drag, the transition to turbulence, and flow separation [1]. Therefore, the capability of measuring both temporally and spatially resolved wall shear stresses is important not only from the standpoint of research on basic fluid mechanics, but also from the perspective of flow control.

Techniques for measuring the shear stress can be categorized into indirect and direct methods [2]. In indirect methods, the shear stress is extracted from the measurement of other flow properties (e.g., pressure and wall temperature) that are related to the shear stress. For example, Pitot tubes such as the Preston tube or Stanton tube use a stream-based distribution of pressure along a flow channel to derive the shear stress [3]–[5]. The major disadvantage of the Pitot tube method is that using the ports for pressure measurements requires modification to the wall, presenting a potential disturbance to the flow. Another common indirect method is the "hot film technique" which is based on the thermal transfer principle [6]–[9]. Compared with Pitot tube measurement techniques, thermal sensors cause less disturbance to the flow because the sensor is mounted flush with the surface. However, they suffer from severe sources of error due to interference arising from surrounding humidity and temperature.

Considering the limitations of indirect methods, which strongly depend on empirical laws [2], direct methods are more accurate for measuring shear stress in complex, difficult-to-model flows [10]. Direct measurement relies on detecting the total amount of viscous drag that a surface-mounted force sensor experiences. An example of the direct measurement method is the floating element (FE) sensor, which is based on measuring the displacement of a FE that is flush with the flow. Capacitive [11]–[14] and piezoresistive [15], [16] techniques as well as surface acoustic wave devices [17], [18] have been developed and used to measure the displacement of a FE. However, shear stress sensors fabricated by micromachining have not yet received sufficient validation in a turbulent flow environment, so further advancement is needed to obtain reliable, high-resolution shear stress measurements that are applicable to a wide range of flows. Moreover, piezoelectric (PE) bending structures are known with simple structure and high sensitivity in displacement measurement [19]; however, there is no report on using PE bending structure for shear stress sensing.

This paper details a low-cost small PE floating-element-type sensor (10 mm $\times$ 10 mm $\times$ 20 mm) that was developed using relatively facile techniques. A PMN–33%PT crystal was used in the sensor for its high PE coefficient ($d_{31} = -1330$ pC/N) [20], [21]. The proposed sensor was specifically designed to be both resilient against normal stresses that are generated from the vortex lift-up in the wind tunnel, and to prevent potential errors due to misalignments between the FE and the test plate. Finally, deflection of the PE sensing element was observed in wind tunnel testing. The static shear stress amplitude, that is the low frequency component of the shear stress, was determined

Manuscript received June 22, 2016; revised September 21, 2016; accepted October 23, 2016. Date of publication November 29, 2016; date of current version August 9, 2017. This work was supported by the National Aeronautics and Space Administration under Contract # NNX14AN42A.

T. Kim, A. Saini, J. Kim, A. Gopalarathnam, Y. Zhu, and X. Jiang are with the Department of Mechanical and Aerospace Engineering, North Carolina State University, Raleigh, NC 27695 USA (e-mail: tkim8@ncsu.edu; asaini2@ncsu.edu; jkim50@ncsu.edu; agopalar@ncsu.edu; yzhu7@ncsu.edu; xjiang5@ncsu.edu).

F. L. Palmieri and C. J. Wohl are with the NASA Langley Research Center, Hampton, VA 23681 USA (e-mail: frank.l.palmieri@nasa.gov; c.j.wohl@nasa.gov).

Color versions of one or more of the figures in this paper are available online at http://ieeexplore.ieee.org.

Digital Object Identifier 10.1109/TIE.2016.2630670

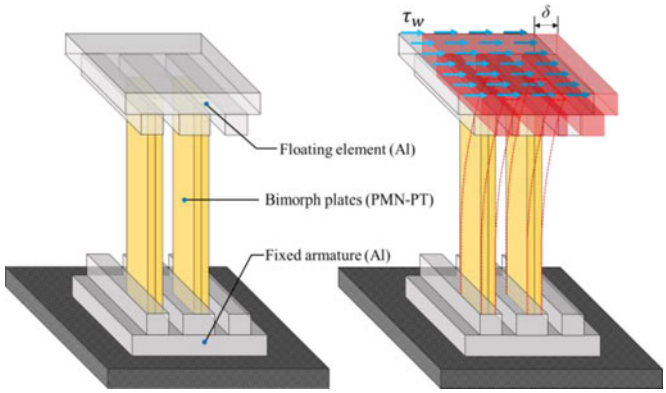

Fig. 1. Schematic of FE sensor: (left) no displacement of FE under the no flow condition and (right) displacement of FE in the application of shear stress.

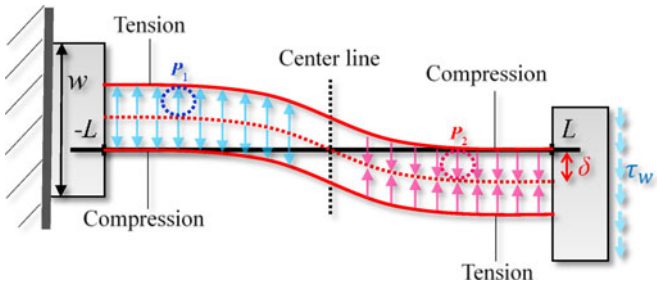

Fig. 2. Configuration of deflected bimorph structure.

through analytical modeling (cantilever beam theory) of the change in resonance frequency of the PE sensing element that would arise from deflection. The variation in charge output from the PE sensor was utilized to determine the dynamic shear stress under the turbulent flow condition.

In this paper, the sensor design and fabrication are described (see Section II). Experimental methods are presented and a dynamic calibration setup for the sensor and the wind tunnel model is illustrated in Section III. Based on this experimental configuration, an analytical model for static stress is proposed and additional devices such as trip-strips and Pitot tubes are introduced for dynamic stress measurement. In Section IV, results are presented, which include the characterization of the fabricated sensor and discussion of static and dynamic stress measurements. Finally, we conclude this paper with a brief summary in Section V.

II. Sensor Design and Fabrication

The direct PE effect was used to sense the displacement of an FE for direct measurement of shear stress. As illustrated in Fig. 1, the FE shifts when flow shear force is applied. The displacement (δ) of the FE causes the bimorph PE structures to deflect, generating an electric charge through the transverse PE coupling (quantified by the coefficient, d_{31}), of the PE plates. The use of at least two parallel bimorphs allows the displaced, FE to move parallel to the fixed armature, preventing any rotation of the sensing armature that could disrupt the flow.

Under a shear stress load, the PE bimorphs bend as shown in Fig. 2. A shear stress is converted into a double-flexion deformation of the bimorphs. The tension and compression stresses are

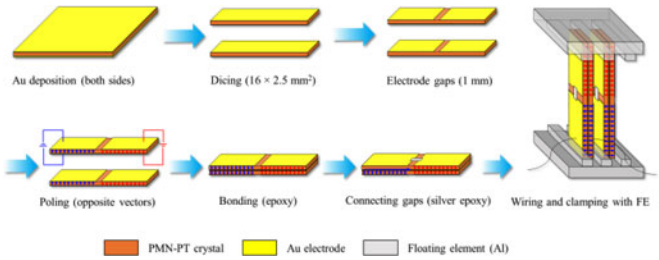

Fig. 3. Sensor fabrication procedure.

then distributed in the PE bimorph. The center of the bimorph corresponds to an inflection point where the stresses vanish. Due to the double-flexion strain caused by clamping, an alternative poling of each plate is necessary to prevent the electrical charge output from cancelling out. This method involves each PE plate being divided into two parts, in which the poling vectors P_1 and P_2 have opposite signs.

The measured displacement of the FE (2δ) and the charge output (Q) can be used to calculate the shear stress and the sensitivity of the sensor, respectively, from the governing equation of the PE effect [22], [23], which is fully derived in a previous publication [24]

$$\begin{bmatrix} 2\delta \\ Q \end{bmatrix} = \begin{bmatrix} \dfrac{s_{11}^E L^3}{wh^3} & -\dfrac{3d_{31}L^2}{4h^2} \\ -\dfrac{3d_{31}L^2}{4h^2} & \dfrac{Lw}{h}\left(\varepsilon_{33}^T - \dfrac{d_{31}^2}{4s_{11}^E}\right) \end{bmatrix} \begin{bmatrix} F \\ V \end{bmatrix} \tag{1}$$

where s_{11}^E is the elastic compliance at a constant electric field, w, h, and L are the width, height, and length of bimorph structure, and d_{31} and ε_{33}^T are the PE and dielectric constants, respectively. V is the voltage and F is the shear force accumulated from the shear stress distributed on the surface of the FE ($F = \tau_w \bullet A_{FE}$), which can be calculated using the measured displacement of the FE based on (1). Finally, the calibrated sensitivity should be

$$S_{cal} = \frac{Q}{\tau_w}(V = 0) = -\left(\frac{3d_{31}L^2}{4h^2}\right) \cdot A_{FE} \tag{2}$$

where A_{FE} is the area of FE.

The FE sensor was fabricated to be small in size (10 mm × 10 mm × 20 mm). The detailed fabrication procedure is presented in Fig. 3. Gold electrodes were deposited on the PMN–33%PT before it was diced (16 mm × 2.5 mm). In order to apply opposite poling vectors to the plates, gaps (1 mm) were formed in the middle of the electrodes on the top and bottom side of plates. Then, poling voltage up to 10 kV/cm was applied to the one end of plate by increasing the voltage step-by-step (0.1 kV/cm) with a high voltage power supply (ValueTronics, Elgin, IL) and staying in connection for 30 min at the desired poling voltage (10 kV/cm). The same procedure was repeated on the other end of plate, but flipping the plate to apply the opposite direction of poling voltage. Finally, two of poled plates were bonded as series mode bimorphs using an epoxy resin (Epotek 301), which ensured the higher sensitivity of the sensors in comparison with the parallel mode connection [22]. The measured *P–E* hysteresis loop of PMN–33%PT is shown in Fig. 4.

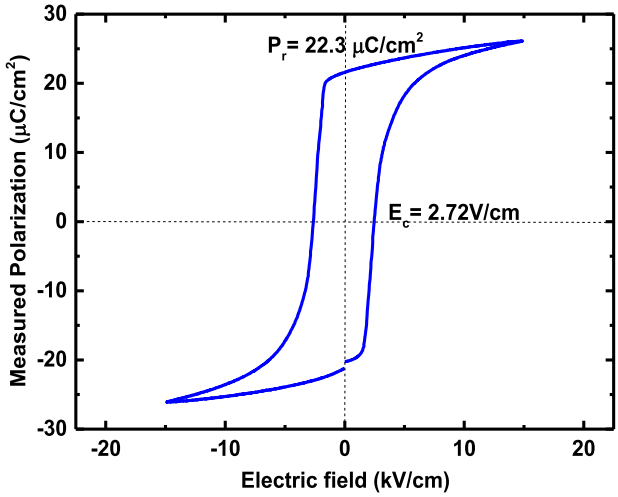

Fig. 4. *P–E* hysteresis loop of PMN–33%PT.

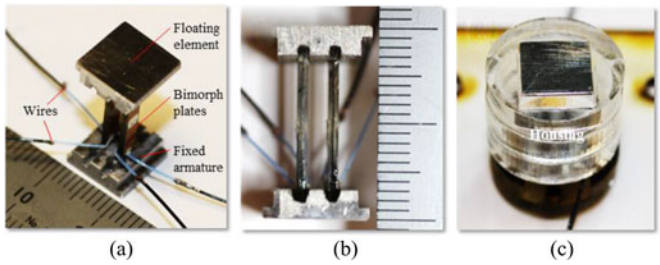

Fig. 5. Configuration of PE sensor: (a) isometric, (b) front view, (c) and with housing. Demarcation on the ruler included in images (a) and (b) is in millimeter.

TABLE I
DIMENSION OF THE PE SENSOR

Bimorph structure			FE
w (mm)	L (mm)	h (mm)	A_{FE} (mm^2)
2.5	16	0.5	10×10

The final prototype of the sensor consists of the FE (top), the clamped element (bottom) with an aluminum plate, two bimorph plates of PMN–33%PT crystals in a series combination, and a protective housing (see Fig. 5). The dimension of PE sensor is listed in Table I.

Another important consideration taken into account during the design of the FE type sensors was the presence of errors caused by sensor misalignments. Misalignment errors originate from the geometry of the FE and the gap surrounding it. When the element is misaligned, pressures acting on the lip and surface of the element create moments which erroneously become part of the wall shear measurement [25]. Some comprehensive studies on misalignment error have been conducted by Allen [26], [27] in which they state that while a perfectly aligned FE would have minimal error, optimizing different geometric parameters could effectively reduce the errors caused by misalignment. They identified three key geometric parameters: misalignment (Z), gap size (G), and lip size (L). These parameters are illustrated in Fig. 6. To prevent or/and

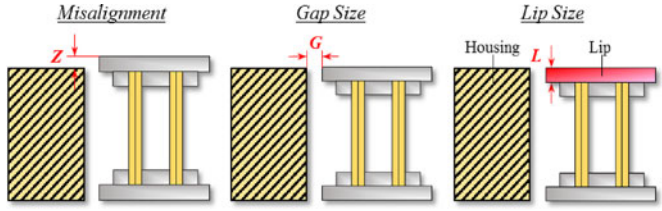

Fig. 6. Key parameters of the FE to minimize the potential errors.

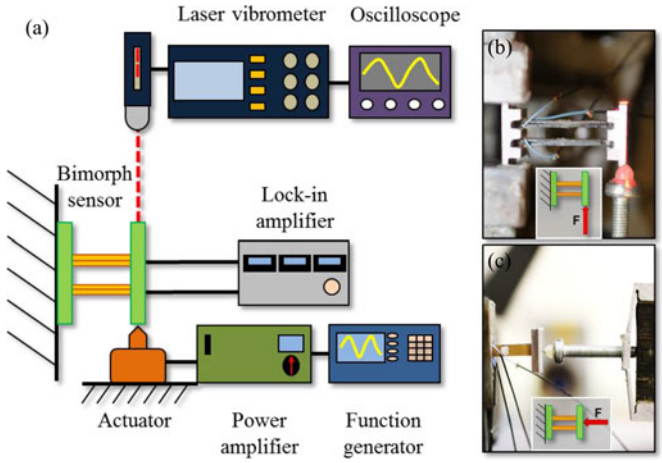

Fig. 7. Experimental setup for the calibration of a sensor in (a) overall view, (b) shear stress, and (c) normal stress.

minimize likely errors from the misalignment between the FE and the test plate, several design considerations were taken into account for the sensors generated in this work [25]–[28].

1) The protective housing. A protective collar component surrounding the FE, if carefully aligned with the FE, can significantly mitigate the effects associated with the sensor misalignment (Z) during a facility installation.
2) Gap size (G) between the FE and housing (200 μm). A sensor with a small gap size is much more prone to misalignment error. The optimum ratio of gap (G) to length of FE was found to be 0.02 through the experimental validation.
3) Lip size (L) of the FE. This was intentionally minimized (1 mm) based on the total height of the FE (3 mm) to reduce the area on which the pressures had to act in the case of misalignment.

III. Experimental Methods

A. Dynamic Calibration

A calibration stage was assembled to characterize the fabricated sensor. Fig. 7(a) represents the experimental setup for the dynamic calibration of the sensor. The actuator, excited by a function generator (Tektronix, Cary, NC) and power amplifier (ValueTronics, Elgin, IL), applied a low frequency (1 Hz) vibrational displacement to the sensor. A laser vibrometer (Polytec, Mooresville, NC) was used to measure the displacement of the FE, while an oscilloscope (Agilent Technologies, Santa Clara, CA) provided a visual display of the displacement profile. The charge output generated from the bimorph PE plate was measured by the lock-in amplifier (Stanford Research Systems,

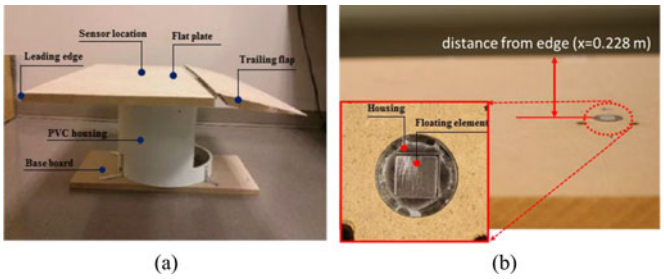

Fig. 8. Wind tunnel experimental setup: (a) side and (b) top and close view.

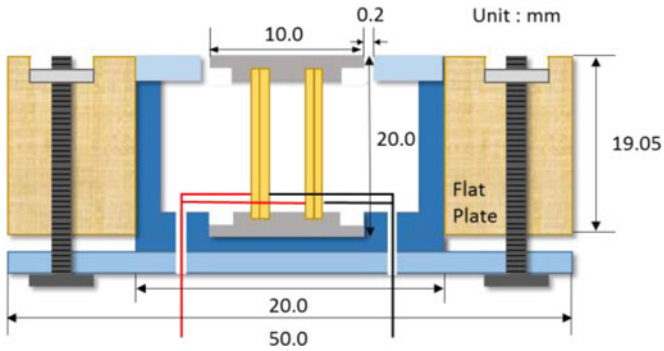

Fig. 9. Schematic of the setup for PE sensor mounted on the test plate.

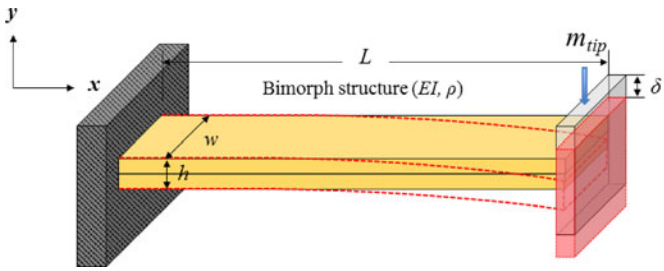

Fig. 10. Cantilever beam with accelerated tip mass.

Sunnyvale, CA). In this test, the reference frequency (1 Hz) of the lock-in amplifier was synchronized with the function generator and the excitation force, i.e., displacement magnitude, was controlled by increasing the voltage amplitude from the function generator in the range of 0.1–1.0 V with a 0.1 V substep. The dynamic calibrations of the shear stress and normal stress were conducted by positioning the contact probe of the actuator on the side and top of the FE [Fig. 7(b) and (c)]. Usable frequency range of the sensor was measured by increasing the reference frequency of the function generator by 1 Hz up to the phase shift of the sensor.

B. Wind Tunnel Model

The characterization of the PE sensors under actual wind-flow conditions was carried out in a subsonic wind tunnel facility at North Carolina State University. The facility enabled an evaluation of the response from PE sensors by comparing the output signals with aerodynamic measurements from several traditional approaches.

The test apparatus was a flat plate fabricated from medium density fiberboard. The flat plate was 406 mm (16″) in chord, 813 mm (32″) in span, and 19.5 mm (¾″) thick. A semicircular leading edge was attached to the front edge of the flat plate, and the PE sensor housing was positioned 229 mm (9″, 0.56 chord) from the leading-edge of the flat plate. Additionally, the flat-plate model had an extended trailing flap attachment. This movable flap enabled adjustments in overall pressure distribution over the flat plate, ensuring that the stagnation point was positioned on the upper surface of the flat plate. Fig. 8 represents the wind tunnel experimental setup for sensors, in which the PE sensor was flush-mounted on the flat plate and carefully aligned by adjustable joint bolts. Fig. 9 shows the schematic of the setup for the PE sensor that was mounted on the test apparatus. Qualitative estimates of the skin friction coefficient and the expected shear stress on the flat plate were conducted using theoretical and experimental boundary layer analysis with the Pitot tube apparatus, which will be introduced in Section III-D in detail.

C. Modeling for Static Stress Measurement

In limited freestream velocity ranges ($< V = 35$ m/s, laminar flow region), the charge output of the PE sensor disappeared after a period of time. Signal vanishing is not appropriate for static stress measurements, so an alternative method that could detect the static stress with the PE sensor was used.

An impedance analyzer (Agilent 4294A, Agilent Technologies, Inc., Santa Clara, CA) was used to measure the variations of resonance frequency due to the deformation of the beam from shear stress. First, lateral mode resonance (f_r) and antiresonance (f_a) frequency were the focused ranges, since the deflection of bimorph plates leads to a change of length in bimorph plates. To analyze resonance frequency shift results using electromechanical modeling, we adopted the cantilever beam theory [29], [30] since the PE bimorph sensor is analogous to a cantilever beam under the same boundary conditions and structures. The central concept of this model is that the shear stress applied to the FE (tip mass) accelerates the tip mass of the beam, which decreases the resonance frequency of the beam (see Fig. 10).

For a cantilever beam subjected to free vibration, the system is considered to be continuous with the beam mass distributed along the shaft. The equation of motion for this can be written as follows [29], [30]:

$$\frac{d^2}{dx^2}\left\{EI\left(x\right)\frac{d^2y\left(x\right)}{dx^2}\right\} = \omega^2 m\left(x\right)y\left(x\right) \tag{3}$$

where E is Young's modulus of the beam material, I is the moment of inertia in the beam cross section, m is the mass per unit length, $m = \rho A$, ρ is the material density, A is the cross-sectional area, x is the distance measured from the fixed end, $y(x)$ is displacement in y direction at distance x from fixed end, and ω is the angular natural frequency. Boundary conditions of the cantilever beam are

$$y\left(0\right) = 0,\ y'\left(0\right) = 0, y''\left(L\right) = 0, y'''\left(L\right) = 0. \tag{4}$$

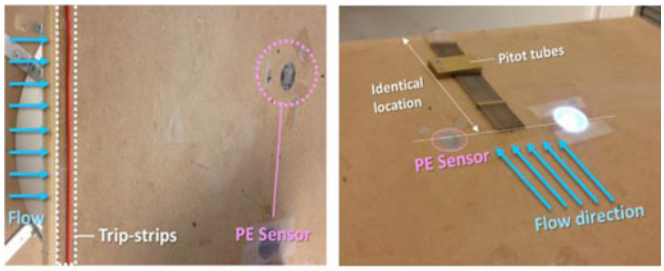

Fig. 11. Experimental setup for (a) tripping the flow to turbulent boundary layer and (b) Pitot tube measurement.

For a uniform beam under free vibration from (3), we obtain

$$\frac{d^4y\left(x\right)}{dx^4}-\beta^4y\left(x\right)=0,\quad \beta^4=\frac{\omega^2m}{\mathrm{EI}}. \tag{5}$$

The mode shapes for a continuous cantilever beam are given as follows:

$$y_n\left(x\right)=A_n\left\{\left(\sin\beta_nL-\sinh\beta_nL\right)\left(\sin\beta_nx-\sinh\beta_nx\right)+\left(\cos\beta_nL-\cosh\beta_nL\right)\left(\cos\beta_nx-\cosh\beta_nx\right)\right\},\quad n=1,\ 2,\ 3\cdots\infty. \tag{6}$$

From (4) and (6), a closed form of the resonance frequency f_n, and the effective mass of beam m_{eff}, without any tip mass can be written as follows:

$$f_n=\frac{1.875^2}{2\pi}\sqrt{\frac{EI}{mL^4}}=\frac{1.875^2}{2\pi}\sqrt{\frac{EI}{\rho AL^4}}=\frac{1}{2\pi}\sqrt{\frac{k}{m_{\mathrm{eff}}}} \tag{7}$$

$$m_{\mathrm{eff}}=\frac{k}{\left(2\pi\cdot f_n\right)^2}=0.2427\,m_{\mathrm{beam}}. \tag{8}$$

Finally, by adding together the tip mass, the mass of the FE, m_{float}, and the effective mass of the beam, the total beam mass, m_{total}, were calculated, and the first flexural mode resonance frequency, $f_{n'}$, in the case of accelerated tip mass was derived:

$$m_{\mathrm{total}}=m_{\mathrm{eff}}+m_{\mathrm{float}}+m_{\mathrm{tip}}=0.2427m_{\mathrm{beam}}+m_{\mathrm{float}}+m_{\mathrm{tip}} \tag{9}$$

$$f_{n'}=\frac{1}{2\pi}\sqrt{\frac{k}{m}}=\frac{1}{2\pi}\sqrt{\frac{3\mathrm{EI}}{\left(0.2427m_{\mathrm{beam}}+m_{\mathrm{float}}+m_{\mathrm{tip}}\right)L^3}}. \tag{10}$$

Next, the applied shear stress on the FE was converted to the accelerated tip mass by using the calibration results and the equation of cantilever beam theory to calculate tip displacement, δ_{tip}

$$\delta_{\mathrm{tip}}=\frac{\tau_wA_{\mathrm{FE}}L^3}{12\mathrm{EI}}=\frac{\mathrm{FL}^3}{12\mathrm{EI}}=\frac{m_{\mathrm{tip}}gL^3}{12\mathrm{EI}} \tag{11}$$

where g is the acceleration of the tip mass. The previous calibration results were used to verify the relationship between the shear stress and deflection of beam. Then, the accelerated tip mass was determined using cantilever beam theory. Finite-element analysis was also performed to verify the resonance frequency shift of the cantilever beam using the commercial FEM package ANSYS.

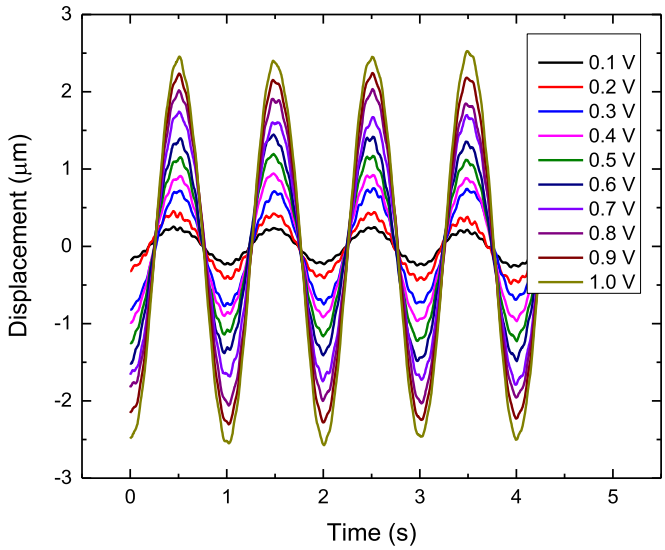

Fig. 12. Peak-to-peak displacement of FE according to voltage amplitudes.

D. Dynamic Stress Measurement

The dynamic stress measurement was performed under turbulent conditions in the wind tunnel. To ensure a turbulent boundary layer at the sensor location, trip-strips were used at a distance in front of the sensor to force the transition to turbulent flow [Fig. 11(a)] [31].

A charge amplifier (output rate, 0.316 mV/pC) and an oscilloscope (20 s window range) were used to ascertain the contributions to the output signal from wind tunnel vibrations; the sensor surface was covered to remove PE FE displacement arising from shear stress. The resultant signal was filtered out from the signal obtained when the PE FE was exposed to the airflow to isolate the shear stress-induced signal.

Simultaneously, a boundary layer analysis with Pitot tubes was conducted to obtain reference shear stress data, and was used for comparing theoretical and experimental values. An experimental setup on the flat plate, consisting of a commercial Pitot tube apparatus (Aerolab LLC, Jessup, MD) with a ten-tap total pressure probe, is presented in Fig. 11(b). The probe was attached on the flat plate at the same distance from the leading edge as the PE sensor. The Pitot tube probes were 1.22 mm apart along the diagonal. Based on the Clauser method [32], [33], which is a common approach for estimating the wall shear stress in turbulent boundary layers, the friction velocity $u_\tau\equiv\sqrt{\tau_w/\rho}$ can be calculated using the measured mean velocity profile $U(y)$ in the logarithmic region of the boundary layer, given by

$$\frac{U\left(y\right)}{u_\tau}=\frac{1}{\kappa}\ln\left(\frac{yu_\tau}{\nu}\right)+B \tag{12}$$

where κ is the von Karman constant (0.41), ν is the fluid kinematic viscosity, and B is the integral constant (5.0) [33]. The wall shear stress can be acquired from the calculated friction

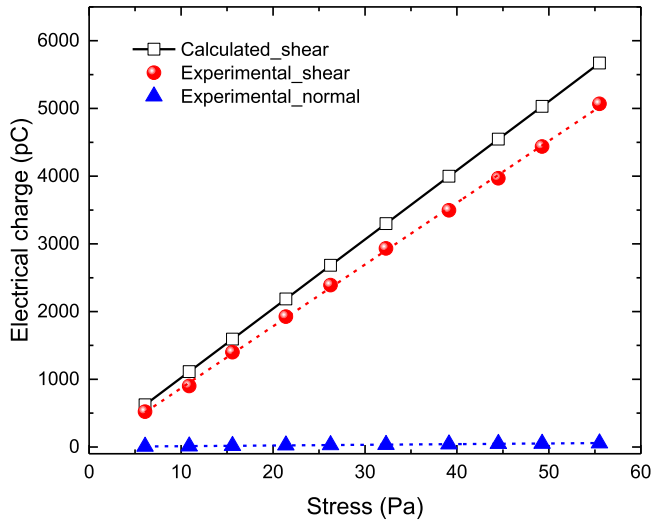

Fig. 13. Calculated (open black squares) and measured electrical charge output as a function of the shear (filled red spheres) and normal stress (filled blue triangles).

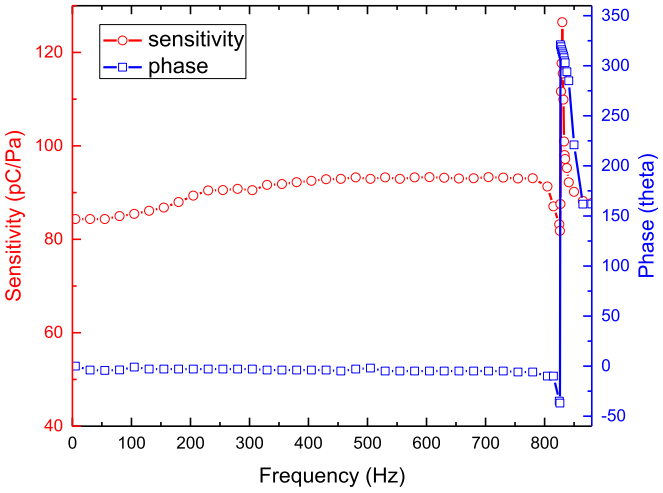

Fig. 14. Usable frequency range of the sensor.

velocity with respect to various freestream velocities from 12 to 28 m/s.

IV. Results and Discussion

A. Dynamic Calibration

Fig. 12 shows the displacement (2δ) of the FE measured from the laser vibrometer as a function of various voltage amplitudes arising from the function generator which were converted into the shear stresses through the actuator based on (1), $\tau_w = \frac{2\delta \cdot w h^3}{s_{11}^E L^3 \cdot A_{\mathrm{FE}}}$.

Calculated and measured electrical charge outputs for the shear and normal stresses are shown in Fig. 13. Measured electrical charge output generated by the shear stress shows an almost linear relationship with respect to the shear stress. Based on a linear fit, $y = 91.29x - 43.7$, the resolution of the sensor was determined to be approximately 0.5 Pa and the operating range of shear stress would be higher

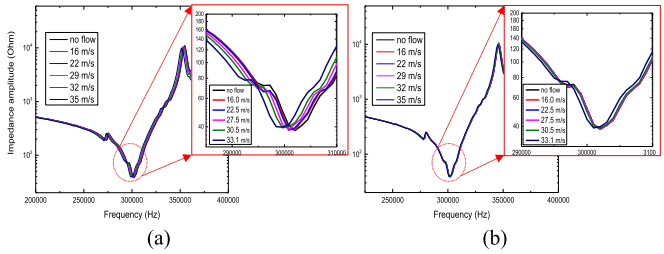

Fig. 15. Variations of frequency under the condition of (a) flow + vibration and (b) vibration only.

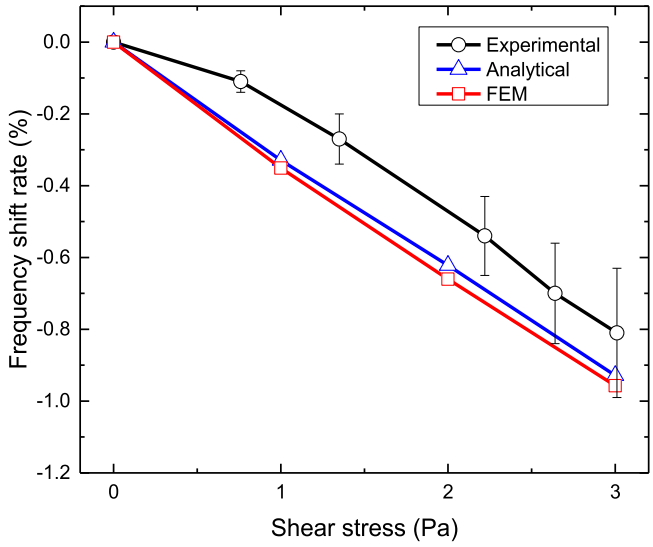

Fig. 16. Comparison between modeled and experimental frequency shift rates.

than 55 Pa. The experimental shear stress sensitivity (91.3 $\pm$ 2.1 pC/Pa) was 10–12% lower than the calculated one ($S_{\mathrm{cal}} = \frac{Q}{\tau_w} = -(\frac{3d_{31}L^2}{4h^2}) \cdot A_{\mathrm{FE}} = 102.1$ pC/Pa), which may be caused by inaccurate PE constants used in the calculation and the clamp effects from the bonded two PE layers to form a bimorph and the bonding of the two ends to the fixed armature and the FE. However, comparing with a sensitivity of the previous work [22], the proposed PE sensor exhibits more than four times higher sensitivity. The high shear stress sensitivity was likely due to a high PE charge constant ($d_{31} = -1330$ pC/N) of PMN–33%PT single crystal [20], [21] and the small thickness of bimorph plates ($h = 0.5$ mm). The sensor yielded an almost zero charge output under normal stress (about 1–1.3% of the shear sensitivity), which was well aligned with the theoretical expectation that the normal stress-induced charge should be approximately zero due to the electromechanical symmetry of bimorph plates. The usable frequency range of the sensor was also determined to be ~800 Hz (see Fig. 14), which indicated that the sensor had a broad-band usage under the turbulent flow condition.

B. Static Stress Measurement

Under the static shear stress condition, Fig. 15 represents the variations of frequency as a function of flow velocity under both

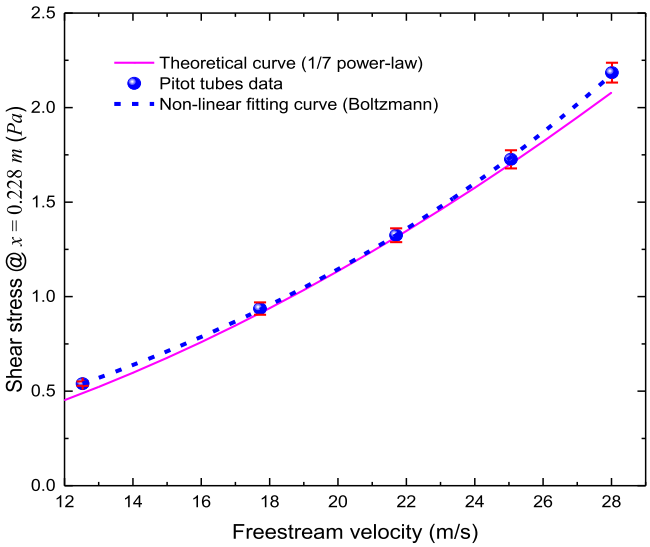

Fig. 17. Comparison in the shear stress between the Pitot tubes measurement and the theoretical analysis.

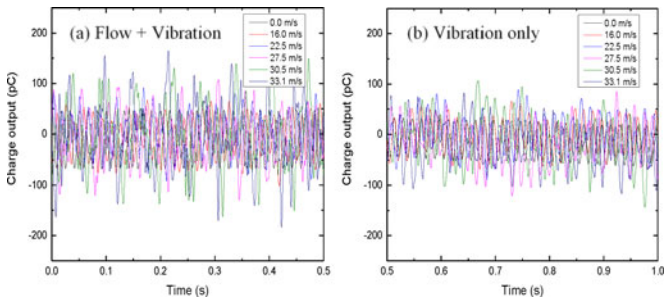

Fig. 18. Charge outputs for dynamic stress in the cases of (a) flow + vibration and (b) vibration only.

the flow and vibration existing condition and the vibration only condition. The resonance frequency shift rate is much higher under the flow and vibration condition (-1.1%) than under the vibration only condition (-0.3%) when compared at the condition of the highest velocity (35 m/s).

Based on the analytical and simulated results of the cantilever beam model, a comparison of frequency shift rates with the experimental results is shown in Fig. 16. With the vibration effect filtered out, the experimental results showed a lower frequency shift rate than the analytical and simulated models (root-mean-square (RMS) error of 13.7%), which may come from damping that occurs in the real device that is not included in the models. However, the results demonstrated consistency between the two frequency shift rates in the overall trend.

C. Dynamic Stress Measurement

The result of the boundary layer analysis utilizing data collected from the Pitot tube device is shown in Fig. 17. A nonlinear curve fitting with the Boltzmann model was conducted on the measured data in which the adjusted *R*-squared value is 0.9936. Furthermore, the result of a fitted line supports the theoretical shear stress curve which is calculated using the 1/7 power law [34].

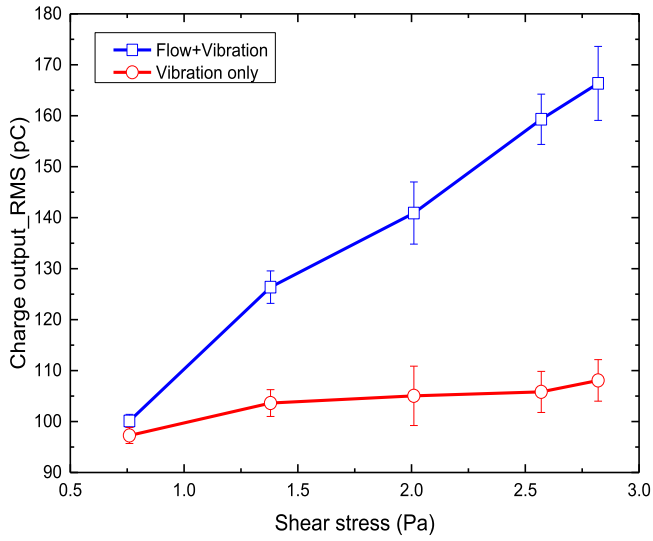

Fig. 19. RMS charge outputs between cases #1 and #2.

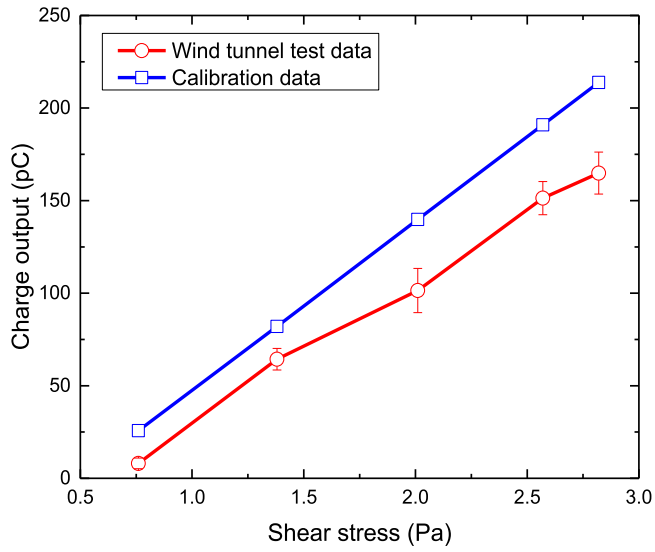

Fig. 20. Comparison in charge outputs between test and calibration data.

Based on the dynamic stress experimental setup, the shear stress effect on the sensor was verified under turbulent flow conditions by comparing the peak-to-peak charge outputs of condition #1 (flow + vibration) and condition #2 (vibration only). As the freestream velocity increased, peak-to-peak charge outputs at both conditions also increased. However, higher peak-to-peak charge outputs were observed under condition #1 relative to condition #2, which indicated that the sensor was able to detect the dynamic shear stress, albeit convolved with signals arising from wind tunnel vibrations (see Fig. 18).

To deconvolute the dynamic shear stress from the vibrational contributions, five datasets were used for each air speed condition with a time window as 20 s. The RMS charge output was determined for each condition. Fig. 19 shows the differences in RMS charge output between cases, which indicated that the PE sensor could detect dynamic shear stress. Considering the vibration only induced sensor's sensitivity as the noise

signal, the signal-to-noise ratio (SNR) can be calculated as 15.8 $\pm$ 2.2 dB, which indicates the competitive performance of the sensors.

To get the pure shear stress data, we filtered out the vibration induced noise by subtracting the vibration charge outputs, which is shown in Fig. 20.

Compared with dynamic calibration data, wind tunnel test data exhibited lower charge outputs, approximately 20–27%, than those obtained in the calibration experiments. This suggests that the wind tunnel vibrational contribution to the signal may reduce the sensitivity of the sensor. The frequency spectrum of vibration in the sensor higher than 800 Hz may cause the sensor performance to degrade. However, sensitivity of the sensor remains high (56.5 $\pm$ 4.6 pC/Pa), and when considering various uncontrollable parameters in the wind tunnel, such as temperature and vibration, it presented comparable results.

V. Conclusion

In this paper, a PE FE type shear stress sensor was developed, calibrated, and tested in a wind tunnel. The sensor was designed to minimize misalignment error by using a protective housing, optimizing the gap size, and minimizing the lip size. The sensor was also designed to be resilient against normal stresses generated from the vortex lift-up so that pure shear stress could be measured. The calibration results showed that the sensor yielded high shear stress sensitivity due to the high PE charge constant (d_{31}) of the PMN–33%PT single crystal and small thickness of the plates, while showing minimal sensitivity to normal stress. In subsonic wind tunnel tests, electromechanical modeling was performed based on the cantilever beam theory for verifying the results of the resonance frequency shift under the static stress condition. The sensor was found to have an SNR of 15.8 $\pm$ 2.2 dB and a high sensitivity of 56.5 $\pm$ 4.6 pC/Pa in the turbulent flow.

References

[1] A. J. Smits and J. P. Dussauge, *Turbulent Shear Layers in Supersonic Flow*, 2nd ed. New York, NY, USA: Springer, 2006.

[2] J. H. Haritonidis, *Advances in Fluid Mechanics Measurements*, vol. 45. Berlin, Germany: Springer, 1989, pp. 229–261.

[3] J. P. Preston, "The determination of turbulent skin friction by means of pitot tubes," *Aeronaut. J.*, vol. 58, no. 518, pp. 109–121, Feb. 1954.

[4] J. N. Hool, "Measurement of skin friction using surface tubes," *Aircr. Eng. Aerosp. Technol.*, vol. 28, no. 2, pp. 52–54, Dec. 1956.

[5] L. F. East, "Measurement of skin friction at low subsonic speeds by the razor-blade technique," *Aeronaut. Res. Council*, no. 3525, pp. 1–24, Aug. 1966.

[6] J. H. Haritonidis, "The fluctuating wall-shear stress and the velocity field in the viscous sublayer," *Phys. Fluids*, vol. 31, pp. 1026–1033, Jan. 1988.

[7] M. Laghrouche, L. Montes, J. Boussey, D. Meunier, S. Ameur, and A. Adane, "In situ calibration of wall shear stress sensor for micro fluidic application," *Procedia Eng.*, vol. 25, pp. 1225–1228, Sep. 2011.

[8] C. Liu *et al.*, "A micromachined flow shear-stress sensor based on thermal transfer principles," *J. Microelectromech. Syst.*, vol. 8, no. 1, pp. 90–98, Mar. 1999.

[9] A. Etrati, E. Assadian, and R. B. Bhiladvala, "Analyzing guard-heating to enable accurate hot-film wall shear stress measurements for turbulent flows," *Int. J. Heat Mass Transf.*, vol. 70, no. 80, pp. 835–843, Mar. 2014.

[10] J. A. Schetz, "Direct measurement of skin friction in complex fluid flows," *AIAA J.*, vol. 44, pp. 1–28, Jan. 2010.

[11] A. Padmanabhan, H. Goldberg, K. D. Breuer, and M. A. Schmidt, "A wafer-bonded floating-element shear stress microsensor with optical position sensing by photodiodes," *J. Microelectromech. Syst.*, vol. 5, no. 4, pp. 307–315, Dec. 1996.

[12] W. D. C. Heuer and I. Marusic, "Turbulence wall-shear stress sensor for the atmospheric surface layer," *Meas. Sci. Technol.*, vol. 16, pp. 1644–1649, Jul. 2005.

[13] J. Zhe, V. Modi, and K. R. Farmer, "A microfabricated wall shear-stress sensor with capacitative sensing," *J. Microelectromech. Syst.*, vol. 14, no. 1, pp. 167–175, Feb. 2005.

[14] A. V. Desai and M. A. Haque, "Design and fabrication of a direction sensitive MEMS shear stress sensor with high spatial and temporal resolution," *J. Micromech. Microeng.*, vol. 14, no. 12, pp. 1718–1725, Sep. 2004.

[15] K. Y. Ng, J. Shajii, and M. A. Schmidt, "A liquid shear-stress sensor fabricated using wafer bonding technology," *J. Microelectromech. Syst.*, vol. 1, pp. 89–94, Jun. 1991.

[16] H. D. Goldberg, K. S. Breuer, and M. A. Schmidt, "A silicon wafer-bonding technology for microfabricated shear-stress sensors with backside contacts," in *Tech. Dig. Solid-State Sens. Actuator Workshop*, vol. 1, Jun. 1994, pp. 111–115.

[17] Y. R. Roh, "Development of local/global SAW sensors for measurement of wall shear stress in laminar and turbulent flows," Ph.D. dissertation, Dept. Mech. Eng., Penn. State Univ., State College, PA, USA, Aug. 1991.

[18] D. Roche, C. Richard, L. Eyraud, and C. Audoly, "Shear stress sensor using a shear horizontal wave SAW device type on a PZT substrate," *Ann. Chim. Sci. Mater.*, vol. 20, no. 7, pp. 495–498, Dec. 1995.

[19] V. Mortet, R. Petersen, K. Haenen, and M. D'Olieslaeger, "Wide range pressure sensor based on a piezoelectric bimorph microcantilever," *Appl. Phys. Lett.*, vol. 88, pp. 5–8, Mar. 2006.

[20] R. Zhang, B. Jiang, and W. Cao, "Elastic, piezoelectric, and dielectric properties of multidomain 0.67Pb($Mg_{1/3}Nb_{1/3}$)$O_{3-0.33}PbTiO_3$ single crystals," *J. Appl. Phys.*, vol. 90, no. 7, pp. 3471–3475, Oct. 2001.

[21] S. Zhang, F. Li, X. Jiang, J. Kim, J. Luo, and X. Geng, "Advantages and challenges of relaxor-$PbTiO_3$ ferroelectric crystals for electroacoustic transducers—A review," *Progress Mater. Sci.*, vol. 68, no. 1, pp. 1–66, Mar. 2015.

[22] J. G. Smits, S. I. Dalke, and T. K. Cooney, "The constituent equations of piezoelectric bimorphs," *Sens. Actuators A, Phys.*, vol. 28, no. 1, pp. 41–61, Jun. 1991.

[23] D. Roche, C. Richard, L. Eyraud, and C. Audoly, "Piezoelectric bimorph bending sensor for shear-stress measurement in fluid flow," *Sens. Actuators A: Phys.*, vol. 55, no. 2, pp. 157–162, Jul. 1996.

[24] T. Kim *et al.*, "A piezoelectric shear stress sensor," *Proc. SPIE*, vol. 9803, pp. 1–7, Mar. 2016.

[25] R. J. Meritt and J. M. Donbar, "Error source studies of direct measurement skin friction sensors," *AIAA J.*, vol. 1916, pp. 1–20, Jan. 2015.

[26] J. M. Allen, "Experimental study of error sources in skin-friction balance measurements," *J. Fluids Eng.*, vol. 99, no. 1, pp. 197–204, Mar. 1977.

[27] J. M. Allen, "An improved sensing element for skin-friction balance measurements," *AIAA J.*, vol. 18, pp. 1342–1345, Jan. 1980.

[28] F. B. O'Donnell and J. C. Westkaempfer, "Measurement of errors caused by misalignment of floating-element skin-friction balances," *AIAA J.*, vol. 3, no. 1, pp. 163–165, Jan. 1965.

[29] L. Meirovitch, *Analytical Methods in Dynamics*. New York, NY, USA: Macmillan, 1967.

[30] R. W. Clough and J. Penzien, *Dynamics of Structures*. New York, NY, USA: McGraw-Hill, 1975, pp. 314–317.

[31] R. A. C. M. Slangen, "Experimental investigation of artificial boundary layer transition," Ph.D. dissertation, Dept. Mech. Eng., Delft Univ. Technol., Delft, The Netherlands, Aug. 2009.

[32] H. H. Fernholz and P. J. Finley, "The incompressible zero-pressure-gradient turbulent boundary layer: An assessment of the data," *Prog. Aerosp. Sci.*, vol. 32, no. 4, pp. 245–311, Aug. 1996.

[33] A. Kendall and M. Koochesfahani, "A method for estimating wall friction in turbulent wall-bounded flows," *Exp. Fluids*, vol. 44, no. 5, pp. 773–780, May 2008.

[34] L. J. De Chant, "The venerable 1/7th power law turbulent velocity profile: A classical nonlinear boundary value problem solution and its relationship to stochastic processes," *Appl. Math. Comput.*, vol. 161, no. 2, pp. 463–474, Feb. 2005.

Taeyang Kim received the B.S. degree from the Korea Military Academy, Seoul, South Korea, in 2005, and the M.S. degree from Texas A&M University, College Station, TX, USA, in 2009, both in mechanical engineering.

In 2014, he joined Dr. Xiaoning Jiang's Micro /Nano Engineering Laboratory at North Carolina State University, Raleigh, NC, USA, where he is working on smart materials, structures, and applications. He is also interested in design and fabrication of piezoelectric sensors which are used for shear stress measurement, medical devices, and nondestructive testing.

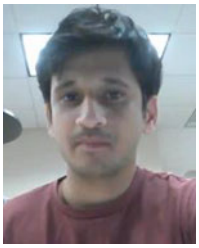

Aditya Saini was born in Faridabad, India. He received the B.Tech. degree in mechanical engineering from the Indian Institute of Technology Ropar, Punjab, India, in 2012. He joined North Carolina State University, Raleigh, NC, USA, for graduate study in 2012 and received the M.S degree in aerospace engineering in 2014. He continued to work in the Applied Aerodynamics Research Group at North Carolina State University and is currently working toward the Ph.D. degree.

Jinwook Kim (S'14) received the B.S. and M.S. degrees in mechanical engineering from Kyungpook National University, Daegu, South Korea, in 2010 and 2012, respectively, working on design and optimization of underwater transducers.

In 2013, he joined Dr. Xiaoning Jiang's Micro /Nano Engineering Laboratory at North Carolina State University, Raleigh, NC, USA, were he is working on the design and fabrication of ultrasound transducers for diagnosis and noninvasive therapy. His broad research interests involve laser-generated ultrasound, ultrasound-mediated therapies, and biosensors.

Ashok Gopalarathnam received the B.Tech. and M.S. degrees from the Indian Institute of Technology Madras, Chennai, India, in 1989 and 1993, respectively, and the Ph.D. degree from the University of Illinois at Urbana-Champaign, Champaign, IL, USA, in 1999, all in aerospace engineering.

He worked on aircraft aerodynamics and design at the National Aerospace Laboratories, Bangalore, India, during 1991–1994, at Scaled Composites in 1998, and as a Consultant to various companies since then. He is currently a Professor of mechanical and aerospace engineering at North Carolina State University, Raleigh, NC, USA, where he leads the Applied Aerodynamics Research Group. His research interests are in applied aerodynamics, including unsteady and post-stall aerodynamic prediction techniques, aerodynamic sensing, aircraft flight mechanics, and design.

Yong Zhu received the B.S. degree in mechanics and mechanical engineering from the University of Science and Technology of China, Hefei, China, in 1999, and the M.S. and Ph.D. degrees in mechanical engineering from Northwestern University, Evanston, IL, USA, in 2001 and 2005, respectively.

He was a Postdoctoral Fellow at The University of Texas at Austin before joining North Carolina State University, Raleigh, NC, USA, in 2007. He is currently an Associate Professor of mechanical and aerospace engineering and an Adjunct Professor of materials science and engineering and biomedical engineering. He is an author or coauthor of four book chapters and 60 peer-reviewed journal papers. His research interests include mechanics of nanomaterials, micro/nanoelectromechanical systems, and flexible/stretchable electronics.

Frank L. Palmieri received the B.S. degree from Virginia Commonwealth University, Richmond, VA, USA, in 2002, and the Ph.D. degree from The University of Texas at Austin, Austin, TX, USA, in 2008, both in chemical engineering.

He is a Research Materials Engineer, AST, in the Advance Materials and Processing Branch of the NASA Langley Research Center, Hampton, VA. He was previously with the National Institute of Aerospace where he focused on high-precision surface chemical and topographical modification for next-generation bonding technologies. In 2008 and 2009, he was with The Photonik Zentrum Hessen, Wetzlar, Germany, working to develop and produce nano-optical components using a nano-imprint lithography technique known as Step and Flash Imprint Lithography (S-FIL). He is an author of more than 20 technical publications and five patents. His research focuses on engineering and interfacial science with applications in the assembly of composite and metallic structures.

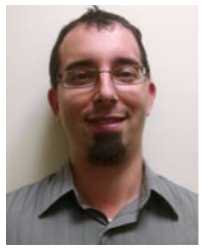

Christopher J. Wohl received the B.S. degree in chemistry from Virginia Polytechnic Institute and State University, Blacksburg, VA, USA, in 2002, and the Ph.D. degree in physical chemistry from Virginia Commonwealth University, Richmond, VA, in 2006.

He is a Senior Research Scientist in the Advanced Materials and Processing Branch of the NASA Langley Research Center, Hampton, VA. He has experience in a variety of fields including physical, polymeric, and organic chemistry, laser spectroscopy, kinetics, and surface and interfacial sciences. He is the author or coauthor of 25 reviewed journal articles, 38 other conference papers, 18 invention disclosures, 10 patent applications, and 2 issued patents. His research focuses on the generation, characterization, and modification of novel materials for adhesion mitigation involving surface engineering and self-organizing systems.

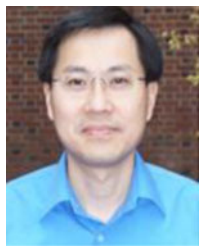

Xiaoning Jiang (SM'11) received the B.S. degree in mechanical engineering from Shanghai Jiaotong University, Shanghai, China, in 1990, the M.S. degree in mechanical engineering from Tianjin University, Tianjin, China, in 1992, and the Ph.D. degree in precision instruments from Tsinghua University, Beijing, China, in 1997.

He received postdoctoral training at Nanyang Technological University and The Pennsylvania State University from 1997 to 2001. He joined Standard MEMS, Inc., as an R&D Engineer in 2001 and then worked for TRS Technologies, Inc., as a Research Scientist, Senior Scientist, Chief Scientist, and Vice President for Technology before joining North Carolina State University, Raleigh, NC, USA, in 2009. He is currently a Professor of mechanical and aerospace engineering and an Adjunct Professor of biomedical engineering. He is the author or coauthor of 5 book chapters, 1 book, 9 issued U.S. patents, more than 74 peer-reviewed journal papers, and more than 80 conference papers on piezoelectric sensors, actuators, transducers, piezoelectric composite micromachined ultrasound transducers, ultrasound for medical imaging and therapy, nondestructive evaluation (NDE), smart materials and structures, flexoelectrics, and micro/nanoelectromechanical systems.

Prof. Jiang is a member of the Technical Program Committee of the IEEE Ultrasonics, Ferroelectrics and Frequency Control Society (UFFC), SPIE Smart Structures/NDE, and ASME International Mechanical Engineering Congress and Exposition. He is also the UFFC representative to the IEEE Nanotechnology Council, and an Editorial Board member of *Sensors*.